Modelling of ultrasound therapeutic heating and numerical study of the dynamics of the induced heat shock response.

Andrzej Mizera[*,a,b], Barbara Gambin[a]

[a] *Institute of Fundamental Technological Research, Polish Academy of Sciences, Pawińskiego 5B, 02-106 Warsaw, Poland*
[b] *Department of Information Technologies, Åbo Akademi University & Turku Centre for Computer Science, Joukahaisenkatu 3-5A, FIN-20520 Turku, Finland*

Abstract

In this presentation we consider *hyperthermia*, a procedure of raising the temperature above 43 °C, as a treatment modality. To this purpose, a numerical model of *in vivo* soft tissue ultrasound heating is proposed by extending a previously presented *in vitro* model. Based on the numerical simulations, a heating scheme satisfying some constraints related to potential clinical applications is established, and the resulting temperature time-course profile is composed with the temperature-dependent protein denaturation formula of a recently published mathematical model for the eukaryotic heat shock response. The obtained simulation results of the combined models are discussed in view of potential application of ultrasound soft tissue heating in clinical treatment.

Key words:
Hyperthermia, Heat Shock Response dynamics, Ultrasound therapeutic treatment, mathematical modelling

1. Introduction

The heat shock response (HSR) is a highly evolutionarily conserved defence mechanism allowing the cell to promptly react to elevated temperature and other forms of environmental, chemical or physical stress. Exposure to shock conditions leads to misfolding of proteins, which in turn accumulate and form aggregates with disastrous effect for the cell. However, damage to cells can initiate one of two opposite responses: either apoptosis, the process of programmed cell death which prevents inflammation in multicellular organisms, or heat shock response which enables recovery and survival of the cell. Thus, these two pathways and the interplay between them have the decisive influence on the biological consequences of the stress. At least two main reasons why the heat shock response has been subject to intense research recently (see Chen et al. (2007); Powers and Workman (2007); Voellmy and Boellmann (2007)) should be mentioned. First, as a well-conserved mechanism, it is considered a promising candidate for deciphering the engineering principles being fundamental for any regulatory network. Second, regardless of their regulatory functions in HSR, heat shock proteins have fundamental importance to many key biological processes. Therefore, profound understanding of the HSR mechanism is hoped to have far-reaching consequences for the cell biology and to contribute to the development of new treatment methods for a number of diseases, e.g. neurodegenerative and cardiovascular disorders, cancer, ageing, see Balch et al. (2008); Liu et al. (2002); Lukacs et al. (2000); Morimoto (2008); Workman and de Billy (2007).

The key part of the heat shock response is an abrupt upregulation of the heat shock proteins which prevent the accumulation and aggregation of misfolded proteins. Two groups of heat shock proteins can be distinguished. Some heat shock proteins are constitutively and ubiquitously expressed in all eukaryotic cells. These proteins are called *heat-shock cognates* and are involved in house-keeping roles, e.g. assist nascent proteins in the establishment of proper conformation, transport (shuttle) other proteins between different compartments inside the cell and participate in signal transduction. The second group contains those which expression is induced by stress. They act as *chaperones*, i.e. help

[*]Corresponding author: A. Mizera, e-mail: amizera@ippt.gov.pl, amizera@abo.fi, tel. +48 22 8261281(414)
Email addresses: amizera@ippt.gov.pl, amizera@abo.fi (Andrzej Mizera), bgambin@ippt.gov.pl (Barbara Gambin)

proteins to maintain their structural integrity or assist the damaged proteins in re-establishment of the functional structure. Moreover, some of them can either act as negative regulators of the apoptotic cascade (Beere (2004)) or aid the apoptotic machinery through their chaperone functions, see Takayama et al. (2003) for the review of this issue. These two functions fulfilled by the heat shock proteins, i.e. protein chaperoning and modulation of survival and death-signaling pathways, make them an attractive therapeutic target, for example in the case of neurodegenerative diseases (Kalmar et al. (2005); Morimoto (2008)) or cancer (Liu et al. (2002); Lukacs et al. (2000); Workman and de Billy (2007)). Furthermore, the heat-induced expression of heat shock protein genes is itself a mechanism of particular interest as it enables the design of heat-responsive gene therapy vectors, cf. Walther and Stein (2009).

In this study we consider hyperthermia, procedure of raising the temperature above 37 °C, as a treatment modality both on the tissue and cellular levels. Theoretically, a properly tuned tempo-spatial temperature distribution in a tissue would lead to a desired heat shock response in the tissue forming cells and, in consequence, enhanced expression of heat shock proteins which are important from the therapeutic point of view. One of the most relevant problems which arise in this context is related to the question whether in the considered type of tissue a controlled and effective application of hyperthermia is practically feasible. The application has to be strictly controlled since it is important to assure that the temperature itself is kept within the therapeutic range, i.e. up to 43 °C. Furthermore, the tissue area and exposure time to heating must be precisely defined in order to activate the finely tuned heat shock response, on which the effectiveness of the treatment depends. The utilization of ultrasonic technique for hyperthermia seems a very promising approach capable of meeting such requirements, cf. Humphrey (2007); Kujawska et al. (2004); ter Haar (2008). Ultrasound irradiation does not stimulate ion activity within the cells, which is an undesired side effect of other irradiation techniques, and is non-invasive, i.e. does not require surgical intervention. Technical improvements of the focused ultrasound ensure the non-invasive and strictly controlled heating of the target tissue volumes. As mentioned before, the control over the spatial temperature distribution in a tissue is of essential importance for the appropriate induction of gene expression on the cellular level. By adjusting the ultrasound beam's intensity, frequency, pulse duration, duty-cycle and exposure time, the proper ultrasonic regime can be tuned. It is now crucial that the research is extended towards the establishment of safe protocols for inducing heat shock response by ultrasound irradiation, which could be applied in clinical treatment.

In Gambin et al. (2009), a very simple Finite Element Method (FEM) model of soft tissue ultrasound heating was introduced. Based on it, a heating scheme satisfying the requirement that the temperature induced by the ultrasound transducer in the focal area does not exceed 43 °C was proposed in Mizera and Gambin (2009). Further, the influence of the tissue heating scheme on the heat shock response measured by the levels of induced free heat shock proteins and misfolded proteins in the cells was discussed. The construction of the soft tissue heating model in Gambin et al. (2009) was based on an *in vitro* experiment performed in order to investigate the possibilities of inducing temperature fields in soft tissues by the use of focused ultrasound. Hence, the heating process only with respect to the material properties was considered and neither perfusion nor metabolic heat generation were incorporated into the numerical model. For a more detailed discussion on the experimental setup and the soft tissue heating model we refer the reader to Gambin et al. (2009) and Mizera and Gambin (2009).

In this presentation, we extend the numerical tissue heating model from Gambin et al. (2009) by additionally taking into account both perfusion and metabolic heat generation (Section 2). The extended model is utilized to establish an ultrasound heating scheme that meets the requirement of not exceeding the temperature of 43 °C at the transducer's focal point. Next, in Section 3, the resulting temperature time-course profile is combined with the heat-induced protein denaturation formula of the basic HSR mathematical model presented in Petre et al. (2009). Further, based on the numerical simulations of the combined models, the dynamics of the response is compared with the outcomes of the model in Mizera and Gambin (2009) and the obtained results are discussed in view of potential application of ultrasound induced soft tissue heating for therapeutic purposes. Finally, in Section 4, we end with some conclusions and suggestions for further work.

2. Numerical model of the soft tissue ultrasound heating

A very simple numerical model of tissue ultrasound heating was presented in Gambin et al. (2009); Mizera and Gambin (2009) and used to compute tempo-spatial temperature fields generated in soft tissues by ultrasound treatment. The model was constructed in accordance with an *in vitro* experiment discussed in Gambin et al. (2009). The schematic illustration of this experiment is given in Fig. 1. In this presentation we extend the model by considering not

only the heating process with respect to material properties, but also by taking into account perfusion and metabolic heat generation in a soft tissue. These modifications make the extended model to reflect the *in vivo* conditions rather than *in vitro*, which was the case of the original model described in Gambin et al. (2009); Mizera and Gambin (2009).

As stated in Gambin et al. (2009), the general bioheat transfer equation in an inhomogeneous thermally anisotropic medium, occupying domain V in the $3D$ real space, may be written as:

$$\rho(\mathbf{x})\, C(\mathbf{x}) \frac{\partial T(\mathbf{x},t)}{\partial t} = \nabla \cdot K(\mathbf{x}) \cdot \nabla T(\mathbf{x},t) + Q_p(\mathbf{x},t) + Q_{int}(\mathbf{x},t) + Q_{ext}(\mathbf{x},t) \qquad \text{for } \mathbf{x} \in V, \tag{1}$$

where T, t, ∇, ρ, C, K, Q_p, Q_{int}, Q_{ext} denote temperature, time variable, gradient vector, density, specific heat, thermal conductivity of a medium (2nd order tensor in our case), heat sources due to perfusion, internal heat generation and external heating (e.g. by irradiation processes), respectively (see Pennes (1948)). The bioheat equations are present in the literature in many different forms, see, e.g., Weinbaum and Jiji (1985).

We state the initial boundary value problem of the Pennes' bioheat equation (Equation (1)) as follows. The medium under consideration consists of two kinds of material occupying domain $V = V_w \cup V_t$, where V_w and V_t are the volumes occupied by water and tissue, respectively (Fig. 2a). The coefficients in Equation (1) depend on $\mathbf{x}$ in the following way:

$$\rho(\mathbf{x}) = \begin{cases} \rho_w & \text{for } \mathbf{x} \in V_w \\ \rho_t & \text{for } \mathbf{x} \in V_t \end{cases}, \qquad C(\mathbf{x}) = \begin{cases} C_w & \text{for } \mathbf{x} \in V_w \\ C_t & \text{for } \mathbf{x} \in V_t \end{cases},$$

$$K = \begin{cases} K_w & \text{for } \mathbf{x} \in V_w \\ K_t & \text{for } \mathbf{x} \in V_t \end{cases}, \qquad K(\mathbf{x}) = K\mathbf{I}, \quad \text{for } \mathbf{x} \in V, \tag{2}$$

where $\mathbf{I}$ denotes the unit second order tensor. The temperature on the boundary ∂V of the domain V is assumed to be constant, namely

$$T(\mathbf{x},t) = 37\,^{\circ}\mathrm{C}, \quad \mathbf{x} \in \partial V. \tag{3}$$

Perfusion and metabolic heat generation have a significant influence on the heating process of a soft tissue *in vivo*. Taking into account these two elements is the main difference between the model presented in Gambin et al. (2009); Mizera and Gambin (2009), which reflects the *in vitro* conditions, and the one discussed in this presentation. We assume in our numerical computations that the perfusion is given by

$$Q_p(\mathbf{x},t) = w_b\, C_b\, (T_0 - T), \tag{4}$$

where w_b is the blood perfusion rate per unit volume of a tissue and C_b is the specific heat capacity of blood (cf. Yuan (2009); Yue et al. (2004)). Q_{int}, the metabolic heat generation per unit volume is assumed to be constant, i.e.

$$Q_{int}(\mathbf{x},t) = q_m. \tag{5}$$

Finally, the external heat Q_{ext} is modelled by heat sources of the total power $0,16$ W. The heat sources are assumed to be produced by the focused acoustic beam and their arrangement inside the tissue, depicted in Fig. 2b, is adopted from Gambin et al. (2009), where it was optimized to fit the experimental results. The total power is assumed to be uniformly distributed over the volume occupied by the heat sources, which results in the power density of approximately 10^6 W/m^3. The numerical values of the constants appearing in the model are presented in Table 1.

Equations (1)–(4) together with the heat sources geometrical distribution provide a well defined boundary-value problem. The soultion to this problem was obtained numerically by utilizing standard Finite Element Method approach. The simulations were performed with use of the Abaqus 6.9 software (DS Simulia Corp.) and the temperature time-course profiles in the neighbourhood of the ultrasound transducer physical focus point (the place of maximal temperature) were considered. Based on these results, a heating scheme satisfying the previously discussed requirement was obtained. First, the heat sources were turned on at the initial temperature of 37 °C (t = 0s). The heating was turned off when the temperature at the considered point reached 43 °C (t = 130s) and the tissue was left to cool to 38 °C. Subsequently, the cooling process was interrupted by turning on the heating again (t = 201s). The last two phases, i.e. cooling and heating, where repeated periodically in order to obtain a temperature time-course profile for 4 hours. The initial heating phase followed by one periodic phase is depicted in Fig. 3.

It is worth noticing that, although the experiment in Gambin et al. (2009) was performed *in vitro*, its schematic illustration (Fig. 1) remains valid in the *in vivo* case. For example, if the tissue that undergoes the treatment is part of an organ in the abdomen, the surrounding water can represent the peritoneal fluid, which covers the organ.

3. The dynamics of the ultrasound induced heat shock response

In order to investigate how the obtained temperature time-course profile influences the heat shock response on the cellular level, the basic mathematical model of the heat shock response in eukaryotic cells, recently presented in Petre et al. (2009), was exploited. The biochemical model consists of three main modules: the dynamic transactivation of the hsp-encoding genes, their backregulation and the chaperone activity of the heat shock proteins. At elevated temperatures proteins tend to misfold and create aggregates. This has disastrous effects on the cell. Hence, in order to survive, the cell under stress has to promptly increase the level of heat shock proteins (HSP) which act as chaperones by interacting with the misfolded proteins (MFP) and helping them to regain the native conformation (PROT). The control over this defence mechanism is exercised through the regulation of the transactivation of the HSP-encoding gene. In order to transactivate transcription, heat shock factors (HSF) trimerize (by transitory forming dimers (HSF_2)) and in this form (HSF_3) bind to the heat shock element (HSE), i.e. the promotor element of the HSP-encoding gene. Once bound ($HSF_3 : HSE$), the gene is transactivated and new heat shock proteins are synthesized. When the amount of chaperones is big enough to cope with the stress, the mechanism is turned off by free HSPs which bind to free HSFs and HSFs that are in complex forms (HSF_2, HSF_3, $HSF_3 : HSE$) by previously breaking the complexes. In consequence, the production of new HSPs is switched off and no new HSF_3s can be formed. The full list of biochemical reactions is given in Table 2. The biochemical model takes into account only well-documented reactions and does not include any "artificial" elements such as experimentally unsupported components or reactions.

An associated mathematical model is obtained by assuming the *law of mass-action* (Guldberg and Waage (1864, 1879)) for the all considered biochemical reactions. The resulting model is in terms of ordinary, first order differential equations, which form the nonlinear dynamical system presented in Table 3. The heat-induced protein denaturation is modelled by adapting the temperature-dependent formula from Peper et al. (1997) for fractional protein denaturation. It is incorporated into the mathematical model in the form of the rate coefficient of protein misfolding (reaction R_{14}), which is given by the following expression:

$$\varphi(T) = (1 - \frac{0.4}{e^{T-37}}) \cdot 1.4^{T-37} \cdot 1.45 \cdot 10^{-5}\ s^{-1}, \tag{6}$$

where T is the numerical value of the temperature of the environment in Celsius degrees. It is valid for $37 \leq T \leq 45$ and is based on experimental investigations presented in Lepock et al. (1993, 1988). For a detailed description of the model we refer the reader to Petre et al. (2009).

Instead of setting the temperature to a constant value as in Petre et al. (2009), we composed the time-dependent temperature profile obtained from the numerical tissue model from Section 2 with the protein denaturation formula (Equation 6). In this way, the basic model from Petre et al. (2009) was adapted for simulation of the cellular defence against ultrasound induced heating. The simulation results in the form of the number concentrations variations in time of the heat shock proteins and misfolded proteins are depicted in Fig. 4 and 5, respectively.

The obtained results for the new *in vivo* model coincide with the outcomes of the model presented in Mizera and Gambin (2009). The ultrasound induced free HSP level (Fig. 4) is significantly higher than the HSP level under the physiological conditions (37 °C, black dashed line in Fig. 4), which is desired from the therapeutic point of view. Moreover, in the new model the average free HSP level, computed alternatingly as the mean of two consecutive top and bottom or bottom and top peak values (red dashed line), is higher than the corresponding average of the outcomes of the model in Mizera and Gambin (2009), where neither perfusion nor metabolic heat generation was considered (blue dashed line). This shows that *in vivo* ultrasound induced heating may be even more efficient than indicated by *in vitro* experimental results.

However, in therapeutic applications, it is very important to control the level of misfolded proteins and keep it low during the treatment. Otherwise, the heating could cause the cells' death rather than stimulate them to self-repair. Hence, in order to assess a heating protocol in view of therapeutic applicability, it is crucial to examine the induced MFP level. The obtained results (Fig. 5) show that under the discussed heating scheme the level of misfolded proteins

evenly oscillates around the reference level obtained under constant 42 °C heating (black dashed line), i.e. except for the initial phase of less than 20 minutes, the reference line coincides with the average calculated as the mean of two consecutive top and bottom (or *vice versa*) MFP time course peaks (red dashed line). As in Mizera and Gambin (2009), the response to constant 42 °C is chosen as the reference on, since the cells are usually capable of surviving in such conditions. Again, although the difference is not as clear as in the case of the HSP level time course, the obtained results for the new *in vivo* model are slightly better than in the case of the *in vitro* model in Mizera and Gambin (2009). After about 20 minutes of treatment, the average for the *in vitro* model (blue dashed line) is above the average of the model with perfusion and metabolic heat generation taken into account. However, as in Mizera and Gambin (2009), alarming is the protein misfolding at the beginning of the treatment. The only improvement which can be observed here with respect to the previous model, is that the peak value of the whole response in the case of the *in vivo* model is lower ($4.5 \cdot 10^4$ instead of $4.7 \cdot 10^4$ misfolded protein molecules).

4. Conclusions and further research

In this presentation hyperthermia was considered as a treatment method. A soft tissue heating model based on the Pennes' bioheat equation presented in Gambin et al. (2009); Mizera and Gambin (2009) was extended by considering two additional elements: perfusion and metabolic heat generation. Further, it was combined with a new mathematical model of the heat shock response in eukaryotic cells recently presented in Petre et al. (2009). The HSR model is formulated in terms of a system of 10 ordinary, first-order, non-linear differential equations. Based on the performed simulations, an ultrasound heating scheme has been proposed.

The obtained heating regime on the tissue level is capable of inducing a rather reasonable, in view of therapeutic application, heat shock response on the cellular level. The assessment of the heating scheme is based on the time course behaviour of the induced levels of free heat shock proteins and misfolded proteins. However, alarming with respect to the MFP level are the first 20 minutes of the response. An improvement could potentially be achieved by exploiting the "self-learning" property of the heat shock response mechanism in the following way. Since numerical simulations of the model in Petre et al. (2009) indicate that the response to a consecutive heat shock is significantly weaker, the presented heating procedure could be preceded by some properly adjusted temperature increase. In consequence, the initial MFP level peaks would be reduced. However, such pre-treatment should be finely tuned in order to minimize the negative influence it would have on the induction of free heat shock proteins level increase, which is essential for the effectiveness of the therapy.

Finally, the presented simulation results reveal that the basic mathematical model from Petre et al. (2009) might not be robust. This may be concluded based on the fact that the model drastically reacts to temperature changes of a relatively high frequency. The dynamics displayed by the HSR model might be unrealistic with respect to the energy resources it would require. Moreover, robustness is a common and rather crucial feature of all biological systems, which is a contrast with the model, that is supposed to reflect a biological mechanism. This issue asks for a more thorough investigation, potentially accompanied by some experimental verifications which would cast some more light on the problem of robustness of the heat shock response machinery.

Acknowledgements

The work was partially supported by the Polish Ministry of Science and Higher Education, grant No. N N518 426936.

References

Balch, W. E., Morimoto, R. I., Dillin, A., Kelly, J. W., 2008. Adapting proteostasis for disease intervention. Science 319, 916–919.

Beere, H. M., 2004. 'The stress of dying': the role of heat shock proteins in the regulation of apoptosis. J Cell Sci 117 (13), 2641–2651.

Chen, Y., Voegli, T., Liu, P., Noble, E., Currie, R., 2007. Heat shock paradox and a new role of heat shock proteins and their receptors as anti-inflammation targets. Inflamm Allergy Drug Targets 6 (2), 91–100.

Gambin, B., Kujawska, T., Kruglenko, E., Mizera, A., Nowicki, A., 2009. Temperature fields induced by low power focused ultrasound in soft tissues during gene therapy. Numerical predictions and experimental results. Archives of Acoustics 34 (4), 445–459.

Guldberg, C., Waage, P., 1864. Studies concerning affinity. C. M. Forhandlinger: Videnskabs-Selskabet i Christiana 35.

Guldberg, C., Waage, P., 1879. Concerning chemical affinity. Erdmann's Journal fr Practische Chemie 127, 69–114.

Humphrey, V. F., 2007. Ultrasound and matter – physical interactions. Progress in Biophysics and Molecular Biology 93, 195–211.
Kalmar, B., Kieran, D., Greensmith, L., 2005. Molecular chaperones as therapeutic targets in amyotrophic lateral sclerosis. Biochemical Society Transactions 33, 551–552.
Kujawska, T., Wjcik, J., Filipczyński, L., 2004. Possible temperature effects computed for acoustic microscopy used for living cells. Ultrasound in Medicine & Biology 30 (1), 93–101.
Lepock, J. R., Frey, H. E., Ritchie, K. P., 1993. Protein denaturation in intact hepatocytes and isolated cellular organelles during heat shock. The Journal of Cell Biology 122 (6), 1267–1276.
Lepock, J. R., Frey, H. E., Rodahl, A. M., Kruuv, J., 1988. Thermal analysis of chl v79 cells using differential scanning calorimetry: Implications for hyperthermic cell killing and the heat shock response. Journal of Cellular Physiology 137 (1), 14–24.
Liu, B., DeFilippo, A. M., Li, Z., 2002. Overcoming immune tolerance to cancer by heat shock protein vaccines. Molecular cancer therapeutics 1, 1147–1151.
Lukacs, K. V., Pardo, O. E., Colston, M., Geddes, D. M., Alton, E. W., 2000. Heat shock proteins in cancer therapy. In: Habib (Ed.), Cancer Gene Therapy: Past Achievements and Future Challenges. Kluwer, pp. 363–368.
Mizera, A., Gambin, B., 2009. The dynamics of heat shock response induced by ultrasound therapeutic treatment. In: 10th Conference on Dynamical Systems - Theory and Applications, DSTA-2009, Łódź, Poland, December 7-10, 2009, Proceedings. Vol. 2. pp. 847–852.
Morimoto, R. I., 2008. Proteotoxic stress and inducible chaperone networks in neurodegenerative disease and aging. Genes Dev 22, 1427–1438.
Pennes, H. H., 1948. Analysis of tissue and arterial blood temperatures in the resting human forearm. Journal of Applied Physiology 1 (2), 93–122.
Peper, A., Grimbergent, C., Spaan, J., Souren, J., van Wijk, R., 1997. A mathematical model of the hsp70 regulation in the cell. Int. J. Hyperthermia 14, 97–124.
Petre, I., Mizera, A., Back, R.-J., 2009. Computational heuristics for simplifying a biological model. In: Ambos-Spies, K., Löwe, B., Merkle, W. (Eds.), Mathematical Theory and Computational Practice: 5th Conference on Computability in Europe, CiE 2009, Heidelberg, Germany, July 19-24, 2009, Proceedings. Vol. 5635 of Lecture Notes in Computer Science. Springer, pp. 399–408.
Powers, M., Workman, P., 2007. Inhibitors of the heat shock response: Biology and pharmacology. FEBS Lett. 581 (19), 3758–3769.
Takayama, S., Reed, J. C., Homma, S., 2003. Heat-shock proteins as regulators of apoptosis. Oncogene 22, 90419047.
ter Haar, G., 2008. The resurgence of therapeutic ultrasound - a 21st century phenomenon. Ultrasonics 48 (4), 233.
Voellmy, R., Boellmann, F., 2007. Chaperone regulation of the heat shock protein response. Adv Exp Med Biol 594, 89–99.
Walther, W., Stein, U., 2009. Heat-responsive gene expression for gene therapy. Advanced Drug Delivery Reviews 61, 641–649.
Weinbaum, S., Jiji, L. M., 1985. A new simplified bioheat equation for the effect of blood flow on local average tissue temperature. Journal of Biomechanical Engineering 107 (2), 131–139.
Workman, P., de Billy, E., 2007. Putting the heat on cancer. Nature Medicine 13 (12), 1415–1417.
Yuan, P., 2009. Numerical analysis of an equivalent heat transfer coefficient in a porous model for simulating a biological tissue in a hyperthermia therapy. International Journal of Heat and Mass Transfer 52, 1734–1740.
Yue, K., Zhang, X., Yu, F., 2004. An analytic solution of one-dimensional steady-state pennes bioheat transfer equation in cylindrical coordinates. Journal of Thermal Science 13 (3), 255–258.

Material	Water	Soft tissue
Density $[kg/m^3]$	$\rho_w = 1000$	$\rho_t = 1060$
Specific heat $[J/(kg\,K)]$	$C_w = 4200$	$C_t = 3800$
Conductivity $[W/(m\,K)]$	$K_w = 0.6$	$K_t = 0.5$

Parameter	Value
Blood perfusion $[kg/(m^3\,s)]$	$w_b = 0.9$
Blood specific heat $[J/(kg\,K)]$	$C_b = 3800$
Metabolic heat gen. $[W/m^3]$	$q_m = 1085$

Table 1: Numerical values for the constants appearing in the tissue model discussed in Section 2.

$$
\begin{aligned}
&2\,\mathrm{HSF} \rightarrow \mathrm{HSF}_2 && (R_1)\\
&\mathrm{HSF}_2 \rightarrow 2\,\mathrm{HSF} && (R_2)\\
&\mathrm{HSF} + \mathrm{HSF}_2 \rightarrow \mathrm{HSF}_3 && (R_3)\\
&\mathrm{HSF}_3 \rightarrow \mathrm{HSF} + \mathrm{HSF}_2 && (R_4)\\
&\mathrm{HSF}_3 + \mathrm{HSE} \rightarrow \mathrm{HSF}_3 : \mathrm{HSE} && (R_5)\\
&\mathrm{HSF}_3 : \mathrm{HSE} \rightarrow \mathrm{HSF}_3 + \mathrm{HSE} && (R_6)\\
&\mathrm{HSF}_3 : \mathrm{HSE} \rightarrow \mathrm{HSF}_3 : \mathrm{HSE} + \mathrm{HSP} && (R_7)\\
&\mathrm{HSP} + \mathrm{HSF} \rightarrow \mathrm{HSP} : \mathrm{HSF} && (R_8)\\
&\mathrm{HSP} : \mathrm{HSF} \rightarrow \mathrm{HSP} + \mathrm{HSF} && (R_9)\\
&\mathrm{HSP} + \mathrm{HSF}_2 \rightarrow \mathrm{HSP} : \mathrm{HSF} + \mathrm{HSF} && (R_{10})\\
&\mathrm{HSP} + \mathrm{HSF}_3 \rightarrow \mathrm{HSP} : \mathrm{HSF} + 2\,\mathrm{HSF} && (R_{11})\\
&\mathrm{HSP} + \mathrm{HSF}_3 : \mathrm{HSE} \rightarrow \mathrm{HSP} : \mathrm{HSF} + \mathrm{HSE} + 2\,\mathrm{HSF} && (R_{12})\\
&\mathrm{HSP} \rightarrow && (R_{13})\\
&\mathrm{PROT} \rightarrow \mathrm{MFP} && (R_{14})\\
&\mathrm{HSP} + \mathrm{MFP} \rightarrow \mathrm{HSP} : \mathrm{MFP} && (R_{15})\\
&\mathrm{HSP} : \mathrm{MFP} \rightarrow \mathrm{HSP} + \mathrm{MFP} && (R_{16})\\
&\mathrm{HSP} : \mathrm{MFP} \rightarrow \mathrm{HSP} + \mathrm{PROT} && (R_{17})
\end{aligned}
$$

Table 2: The simplified model for the eukaryotic heat shock response.

$$
\begin{aligned}
dX_1/dt = &-2k_1^+X_1^2 + 2k_1^-X_2 - k_2^+X_1X_2 + k_2^-X_3 - k_5^+X_1X_6 \\
&+ k_5^-X_7 + k_6X_2X_6 + 2k_7X_3X_6 + 2k_8X_5X_6 && (7)\\
dX_2/dt = &\ k_1^+X_1^2 - k_1^-X_2 - k_2^+X_1X_2 + k_2^-X_3 - k_6X_2X_6 && (8)\\
dX_3/dt = &\ k_2^+X_1X_2 - k_2^-X_3 - k_3^+X_3X_4 + k_3^-X_5 - k_7X_3X_6 && (9)\\
dX_4/dt = &-k_3^+X_3X_4 + k_3^-X_5 + k_8X_5X_6 && (10)\\
dX_5/dt = &\ k_3^+X_3X_4 - k_3^-X_5 - k_8X_5X_6 && (11)\\
dX_6/dt = &\ k_4X_5 - k_5^+X_1X_6 + k_5^-X_7 - k_6X_2X_6 - k_7X_3X_6 \\
&- k_8X_5X_6 - k_{11}^+X_6X_8 + (k_{11}^- + k_{12})X_9 - k_9X_6 && (12)\\
dX_7/dt = &\ k_5^+X_1X_6 - k_5^-X_7 + k_6X_2X_6 + k_7X_3X_6 + k_8X_5X_6 && (13)\\
dX_8/dt = &\ \varphi(T)\,X_{10} - k_{11}^+X_6X_8 + k_{11}^-X_9 && (14)\\
dX_9/dt = &\ k_{11}^+X_6X_8 - (k_{11}^- + k_{12})X_9 && (15)\\
dX_{10}/dt = &-\varphi(T)\,X_{10} + k_{12}X_9 && (16)
\end{aligned}
$$

Table 3: The simplified mathematical model of the heat shock response originally presented in Petre et al. (2009). The model is obtained from the biochemical model shown in Table 2 by assuming the law of mass-action. It is formulated in terms of a system of 10 ordinary, first order, non-linear differential equations. The numerical values of the rate constants, the relationship between the model variables and the metabolites, and initial values of the variables are presented is Table 4.

Param.	Reaction	Value	Unit
k_1^+	(R_1)	3.49	$\frac{V}{\#\cdot s}$
k_1^-	(R_2)	0.19	s^{-1}
k_2^+	(R_3)	1.07	$\frac{V}{\#\cdot s}$
k_2^-	(R_4)	10^{-9}	s^{-1}
k_3^+	(R_5)	0.17	$\frac{V}{\#\cdot s}$
k_3^-	(R_6)	$1.21 \cdot 10^{-6}$	s^{-1}
k_4	(R_7)	$8.3 \cdot 10^{-3}$	s^{-1}
k_5^+	(R_8)	9.74	$\frac{V}{\#\cdot s}$
k_5^-	(R_9)	3.56	s^{-1}
k_6	(R_{10})	2.33	$\frac{V}{\#\cdot s}$
k_7	(R_{11})	$4.31 \cdot 10^{-5}$	$\frac{V}{\#\cdot s}$
k_8	(R_{12})	$2.73 \cdot 10^{-7}$	$\frac{V}{\#\cdot s}$
k_9	(R_{13})	$3.2 \cdot 10^{-5}$	s^{-1}
k_{10}	(R_{14})	$\varphi(T)$	s^{-1}
k_{11}^+	(R_{15})	$3.32 \cdot 10^{-3}$	$\frac{V}{\#\cdot s}$
k_{11}^-	(R_{16})	4.44	s^{-1}
k_{12}	(R_{17})	13.94	s^{-1}

Metabolite	Var.	Init. no.
HSF	X_1	0.669
HSF_2	X_2	$8.73 \cdot 10^{-4}$
HSF_3	X_3	$1.23 \cdot 10^{-4}$
HSE	X_4	29.733
HSF_3 : HSE	X_5	2.956
HSP	X_6	766.875
HSP : HSF	X_7	1403.13
MFP	X_8	517.352
HSP : MFP	X_9	71.648
PROT	X_{10}	$1.15 \cdot 10^8$

Table 4: The numerical values of the rate constants and the initial values of the variables in the simplified mathematical HSR model presented in Petre et al. (2009). The tissue model from Section 2 was combined with the HSR model by composing the protein denaturation coefficient $\varphi(T)$ with the time-dependent temperature profile obtained from the tissue model (Fig. 3). # denotes the number of molecules, V is the cell volume and s - second.

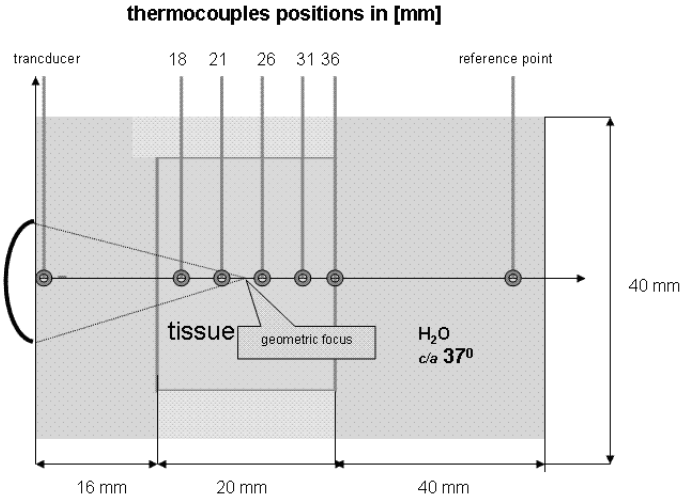

Figure 1: Schematic illustration of the experiment presented in Gambin et al. (2009). 7 thermocouples were used to measure the temperature induced by ultrasound irradiation in various field points along the acoustic axis. The positions are shown in relation to the transducer. In this presentation the temperature in the neighbourhood of the transducer's focal point is considered for establishing the therapeutic heating scheme presented in Fig. 3.

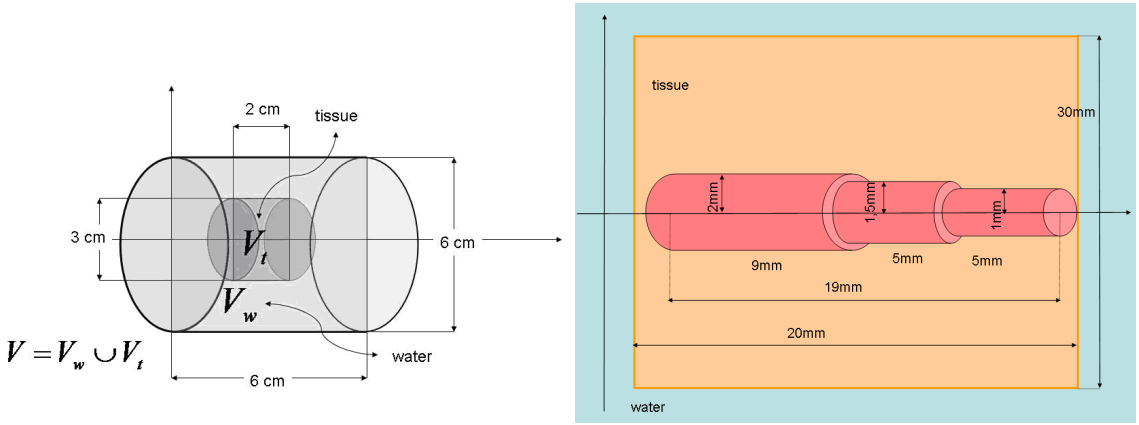

(a) (b)

Figure 2: a) Two domains occupied by water and tissue considered in numerical computations. b) The heat sources geometry assumed in numerical calculations (adopted from Gambin et al. (2009)). The total power of the heat sources is 0.16 W. The power is assumed to be uniformly distributed over the volume occupied by the heat sources ($\approx 10^6$ W/m^3).

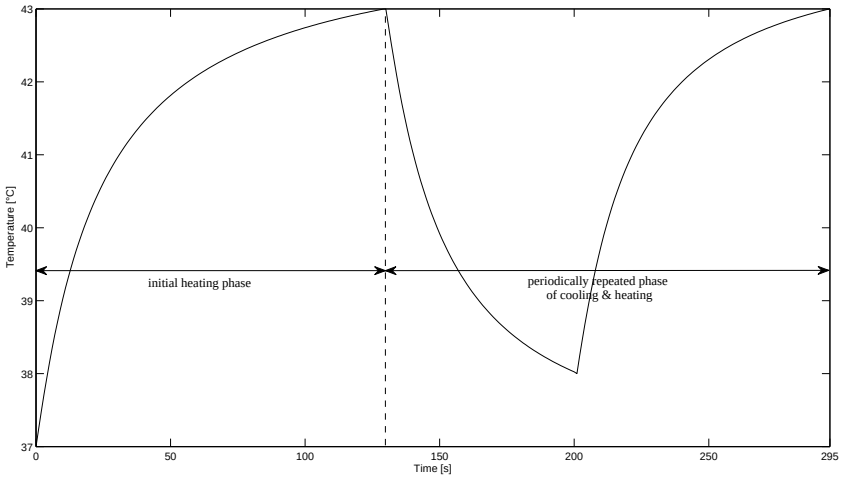

Figure 3: The initial heating phase (0 – 130 s) followed by cooling and heating phase (130 – 295 s). The last phase has been repeated periodically in order to obtain a heating scheme of 4 hours.

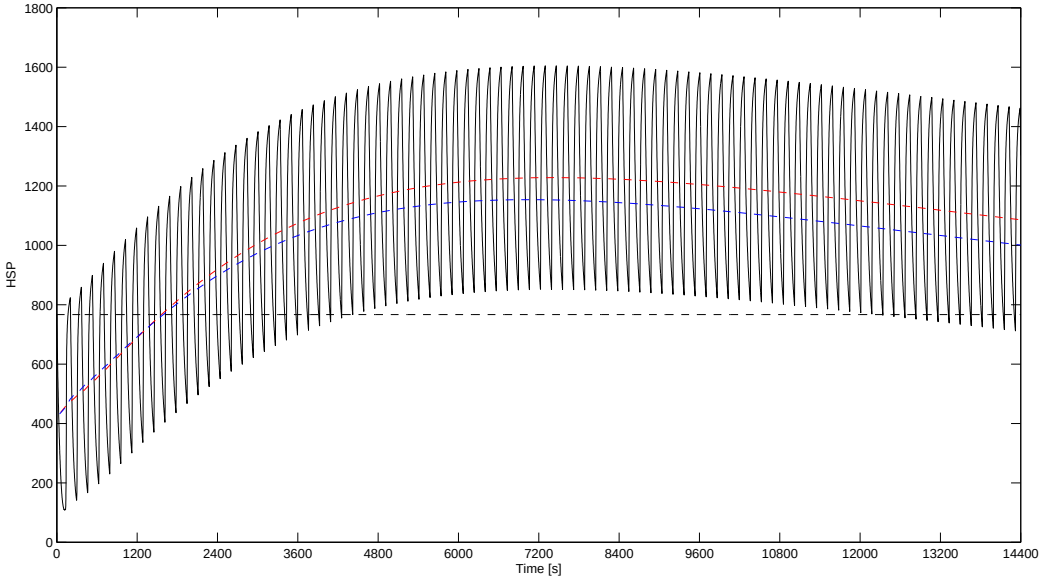

Figure 4: Number of molecules in time of the free heat shock proteins induced by the ultrasound irradiation. The simulation results were obtained by exploiting the basic mathematical model from Petre et al. (2009). The black dashed line indicates the HSP level at physiological conditions (37 °C). The red dashed line is the average obtained by computing the mean values of two consecutive HSP time course peak values (top and bottom or bottom and top, alternatively). Each mean value is placed in the middle of the time interval determined by the two peaks from which the mean value was obtained. The blue dashed line indicates the analogous average for the *in vitro* model presented in Mizera and Gambin (2009).

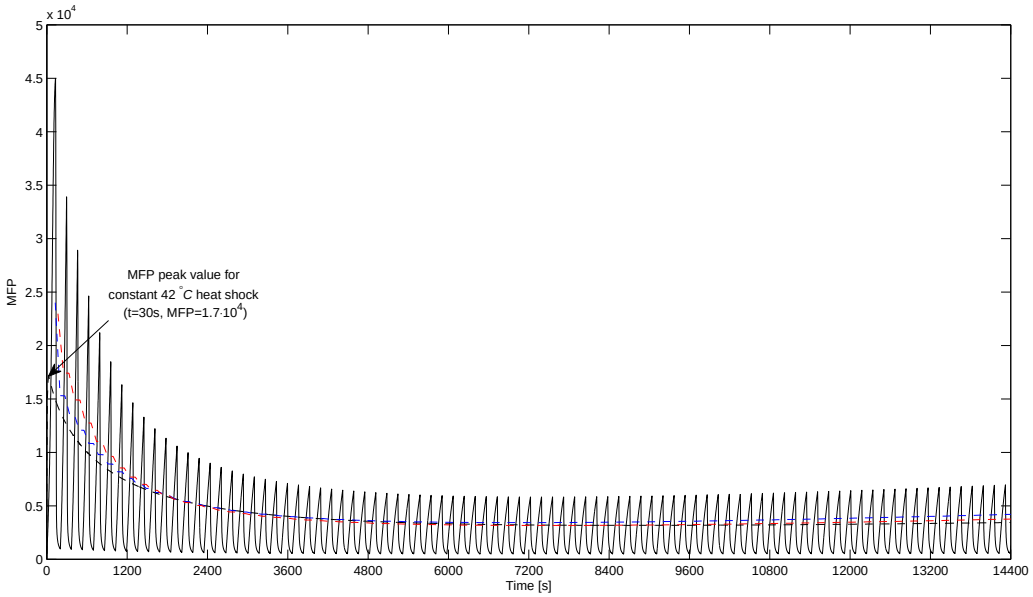

Figure 5: Number of molecules in time of the misfolded proteins induced by the ultrasound irradiation. The simulation results were obtained by exploiting the basic mathematical model from Petre et al. (2009). The black dashed line indicates the MFP level at constant 42 °C heat shock. The red dashed line is the average obtained by computing the mean values of two consecutive MFP time course peak values (top and bottom or bottom and top, alternatively). Each mean value is placed in the middle of the time interval determined by the two peaks from which the mean value was obtained. The blue dashed line indicates the analogous average for the *in vitro* model presented in Mizera and Gambin (2009).